Boundary-Layer Meteorology
https://doi.org/10.1007/s10546-020-00565-2

RESEARCH ARTICLE

Non-local Impacts on Eddy-Covariance Air–Lake CO_2 Fluxes

Leonie Esters[1] · Anna Rutgersson[1] · Erik Nilsson[1] · Erik Sahlée[1]

Received: 2 March 2020 / Accepted: 12 August 2020
© The Author(s) 2020

Abstract
Inland freshwater bodies form the largest natural source of carbon to the atmosphere. To study this contribution to the atmospheric carbon cycle, eddy-covariance flux measurements at lake sites have become increasingly popular. The eddy-covariance method is derived for solely local processes from the surface (lake). Non-local processes, such as entrainment or advection, would add erroneous contributions to the eddy-covariance flux estimations. Here, we use four years of eddy-covariance measurements of carbon dioxide from Lake Erken, a freshwater lake in mid-Sweden. When the lake is covered with ice, unexpected lake fluxes were still observed. A statistical approach using only surface-layer data reveals that non-local processes produce these erroneous fluxes. The occurrence and strength of non-local processes depend on a combination of wind speed and distance between the instrumented tower and upwind shore (fetch), which we here define as the time over water. The greater the wind speed and the shorter the fetch, the higher the contribution of non-local processes to the eddy-covariance fluxes. A correction approach for the measured scalar fluxes due to the non-local processes is proposed and also applied to open-water time periods. The gas transfer velocity determined from the corrected fluxes is close to commonly used wind-speed based parametrizations.

Keywords Air–lake interactions · Carbon dioxide fluxes · Eddy covariance · Non-local processes · Micrometeorology

1 Introduction

Inland freshwater systems such as lakes act as a net source of natural carbon to the atmosphere. The magnitude of the carbon contribution from lakes to the atmosphere is comparable to the open ocean carbon sink (e.g., Cole et al. 2007; Tranvik et al. 2009; Raymond et al. 2013). To study the lake's contribution to the carbon cycle, various methods have been used. Eddy-covariance flux measurements of carbon dioxide (CO_2), and more recently methane (CH_4), have gained popularity (e.g., Eugster et al. 2003; Huotari et al. 2011; Podgrajsek et al. 2014, 2015; Erkkilä et al. 2018; Morin et al. 2018). The eddy-covariance method gives a direct measure of net gas exchange across the air–water interface as long as the lake is within

✉ Leonie Esters
leonie.esters@geo.uu.se

[1] Department of Earth Sciences, LUVAL, Uppsala University, Villavägen 16, 75236 Uppsala, Sweden

Published online: 15 September 2020

the footprint area and other assumptions of the method are fulfilled. In eddy-covariance measurements, the flux is the mean covariance of the fluctuating component of the vertical wind, w, and the fluctuating component of the mixing ratio of interest, c, e.g., $F = \rho_a \overline{w'c'}$. The prime denotes the deviation from the mean, the overbar temporal averaging, and ρ_a is the dry air density. The averaging time should be much longer than the period of any fluctuating motions. The magnitude of conventional averaging periods is 30 min to 1 h (Lee et al. 2005). Deriving this expression for the eddy flux from the conservation equation requires several simplifying assumptions (e.g., Baldocchi and Meyers 1988; Dabberdt et al. 1993; Baldocchi and Vogel 1996; Massman and Lee 2002), and violation of the assumptions can induce errors and uncertainties in the measured flux. One important assumption is that all transport terms in the scalar mass-balance equation are spatially homogeneous. Hence, the atmospheric gas concentration is stationary over the averaging period unless a local source or sink exists. The only accepted source/sink in the system is the respective ecosystem itself, here the lake, and allows us to estimate air–lake fluxes. These assumptions work well for large areas with flat homogeneous terrain. Sahleé et al. (2012) showed that the shape of the turbulence spectra measured above a lake closely resembled shapes expected over adjacent land areas with a reverse atmospheric stability. In complex terrain, the problems of violating these simplifications are well known (e.g., Loescher et al. 2006) and previous results indicate, for example, that forest edges close to the measurement tower are problematic (e.g., Kenny et al. 2017). For lake systems, such violations also need to be investigated. Jammet et al. (2017) found that CO_2 fluxes from a lake were found to be non-zero even when the lake was entirely ice-covered with no branches protruding from of the ice. Hence, CO_2 through holes in the ice was excluded as the origin for the observed CO_2 fluxes (Jammet et al. 2017). From Jammet et al. (2017), it remains unclear whether the fluxes were due to a physical evasion of CO_2 through snow over the lake or due to lateral advection of land-emitted CO_2.

Bruin et al. (1993) hypothesized (and later proved: Bruin et al. 1999) that scalar fluctuations in the atmospheric surface layer over a horizontally, uniform terrain were not only generated by local surface processes but also by non-local ones. Non-local processes comprise large-scale processes such as advection and entrainment. The topographic surroundings of a lake can be the origin for horizontally advected characteristics. Thereby, CO_2 sources from areas outside of the eddy-covariance footprint can be advected to the measurement mast (e.g., Sun et al. 1998; Feigenwinter et al. 2004; Aubinet et al. 2005). Using an analytical approach, Higgins et al. (2013) found that maximal advection occurs when the measuring height is 0.036 times the distance to a land surface transition. Eugster et al. (2003) and Vesala et al. (2006) addressed advection by reducing the averaging window of the eddy- covariance measurements from 30 to 5 min. They argued that when integrating the fluxes, a shorter averaging window eliminates the contribution of the CO_2 flux that most likely originates from the surrounding land. During daytime, the CO_2 uptake over the surrounding land can be stronger than that of the lake. The diurnal CO_2 cycle is typically stronger over land than over the lake during periods with green vegetation due to the cycle in photosynthesis versus respiration (Spank et al. 2019). When lower land-based CO_2 concentration is advected over a lake, the additional sink of CO_2 can be detected as a local downward flux by an installed eddy-covariance system (Sun et al. 1998; Aubinet et al. 2012).

Entrainment is a second potential source of CO_2 within the system. Entrainment can induce scalar characteristics of the above-lying free atmosphere into the boundary layer. The entrained air will affect the characteristics within the boundary layer. The entrained signal can be strong enough to affect the whole boundary layer down to the surface (e.g., Lohou et al. 2010; van de Boer et al. 2014). Entrainment at the top of the planetary boundary layer has a profound influence on the flux imbalance within the boundary layer (Huang et al. 2008). The

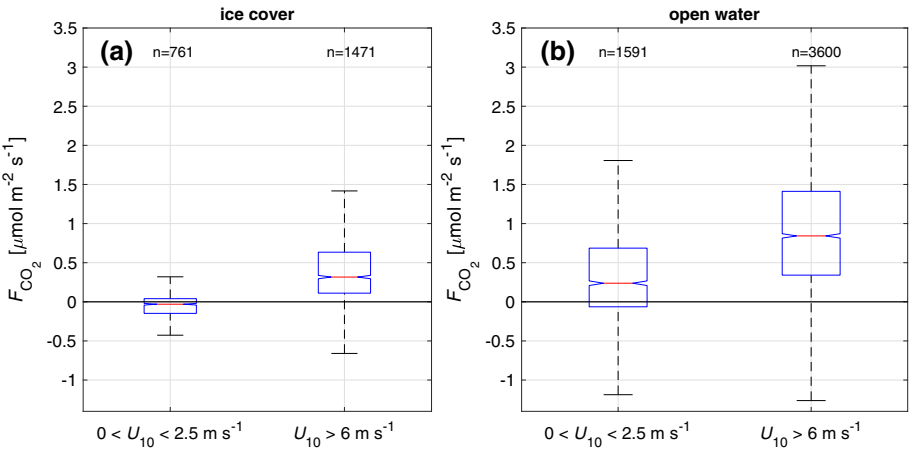

Fig. 1 Boxplots of CO_2 fluxes from four years for **a** periods when the lake was covered with ice and **b** periods when the lake was free of ice. The bottom and top edges of the box indicate the 25th and 75th percentiles, respectively, and the red cental line indicates the median. The upper and lower whiskers are defined by $Q3 + 1.5(Q3 - Q1)$ and $Q1 - 1.5(Q3 - Q1)$ respectively. Here $Q1$ and $Q3$ are the 25th and 75th percentiles

entrainment of warm and dry air from the free atmosphere decreases the similarity between the temperature, T, and specific humidity, q, within the boundary layer (Bruin et al. 1999; Choi et al. 2004; Asanuma et al. 2007; Katul et al. 2008; van de Boer et al. 2014). Under normal conditions, T and q are positively correlated due to the similarity in the heat and water vapour sources at the surface. Entrainment of cold and dry air, however, has been observed to enhance the T–q similarity with increased friction velocity, u_* (Gao et al. 2018). Entrainment cannot be measured directly but must be inferred from other measurements (Lenschow et al. 1999). Based on eddy-covariance measurements at two sites above a fodder and a grass field, van de Boer et al. (2014) presented a statistical method based on the variance of q to detect and quantify entrainment influences on surface-layer measurements.

Eddy-covariance gas fluxes are commonly used to determine the gas transfer velocity, k, via:

$$F_{CO_2} = k s_{CO_2} \Delta P, \tag{1}$$

where F_{CO_2} represents the flux, s_{CO_2} the solubility of CO_2, and ΔP the air–water difference in partial pressure. Thus, too high/low flux estimates can result in an overestimation or underestimation of k. Such incorrect estimates of k lead to uncertainties within empirically derived parametrizations of k. Therefore, they can cause uncertainties in upscaled carbon contributions from lakes to the atmosphere.

Positive (upward) CO_2 fluxes were observed when Lake Erken (see Sect. 2.1), a freshwater lake in mid-Sweden, was covered with ice (Fig. 1). These unexpected fluxes were measured during four winter periods and coincided with moderate to higher wind speeds (above 5 m s^{-1}). The fluxes were smaller than those observed for similar wind speeds during periods when the lake was ice-free. In this study, we will investigate the origin of these unexpected CO_2 fluxes during periods of frozen and open-water conditions. Four years of eddy-covariance observations conducted at the instrumented tower at Lake Erken will be used. We will apply the statistical approach presented by van de Boer et al. (2014) to test the influence of non-local processes on the surface-layer variables, which is described in Sect. 2. Once the origin of

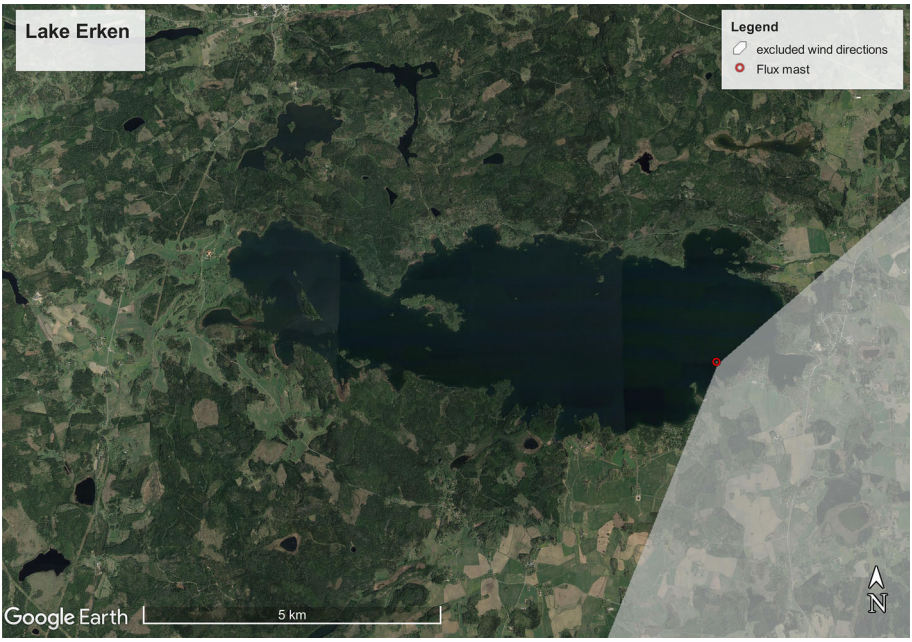

Fig. 2 Google Earth map of Lake Erken showing the surrounding landscape. The flux mast is highlighted by the red circle. The wind directions between 040° and 200°, which are excluded from the presented analysis, are indicated by the overlaying white shade

these fluxes is assessed, we will discuss their impact on the gas transfer velocity (Sect. 3.3) along with the potential implications for other eddy-covariance lake studies (Sect. 4).

2 Methods

2.1 Site and Instrumentation

Measurements were conducted at Lake Erken (59.835° N, 18.633° E), which is located 70 km north-east of Stockholm. Lake Erken has a surface area of 24 km^2, an average depth of 9 m, and a maximal depth of 21 m. The lake's long sides adjoin mixed forest and its shorter sides adjoin agricultural fields and grassland. A permanently staffed biological lab is located at the south-east of the lake. An instrumented tower is installed on Malma Island located close to the south-east shore of the lake. The longest over-lake fetch at the tower is up to 8 km in a direction of 275° and the shortest around 500 m in direction between 200° and 250° (Fig. 2).

The tower was instrumented with measurements of temperature at 1.9 and 6 m above the tower base using ventilated and radiation shielded thermocouples type-T. Wind speed and directions were measured at 2.5 and 6.2 m using propeller anemometers (Young,Wind Monitor, MI, USA). The high frequency instrumentation used in this study for eddy-covariance flux estimates was mounted on a westward facing boom at 4.1 m. This instrumentation consisted of a three-dimensional sonic anemometer (Gill Instruments, Wind Master, Lymington, UK) for the three wind components and temperature. For CO_2 and H_2O measurements, an open

path LI-7500 was used. Sensor separation was measured to 0.3 m, which is expected to give only a small flux loss (Horst and Lenschow 2009; Nilsson et al. 2010). Additionally, the tower was instrumented with sensors recording incoming solar radiation (CS300 Apogee, Silicon Pyranometer, Campbell Sci. Inc., OH, US) from February 2017, and net radiation (CNR-4 Net Radiometer, Kipp & Zonen), air pressure (144SC0811, Sensortechnics GmbH, Puchenheim, Germany), and relative humidity (Rotronic AG, Basserdorf, Switzerland). Aside from the eddy-covariance measurements, the sensors were sampling at 1 Hz and in this study averaged over 30 min. Partial pressure of CO_2 in the water was measured with 30-min time resolution at 0.5 m depth using a Submersible Autonomous Moored Instrument, SAMI2-CO_2 (Sunburst Sensors, MT, USA) during the ice-free season.

Each year was divided into an ice-covered season and an ice-free season. The ice cover was manually recorded by the laboratory staff. During the ice-covered periods, the lake was entirely covered with a thick layer of ice, and no cracks or holes within the ice were observed. During the four years (2015–2018), the lake was covered with ice for a total of 374 days, mainly between January and April.

2.2 Data Processing

The wind speed was measured at the height of 6.2 m and was recalculated with a stability corrected logarithmic profile to 10 m height as U_{10}. Fluxes and variance were determined from the 20-Hz measurements, averaged over 30 min, and subject to double rotation (Kaimal and Finnigan 1994). The data were despiked and linearly detrended. The humidity data were corrected for variations in the air density using the Webb et al. (1980) correction. The time lag caused by the sensor separation between the sonic anemometer and the LI-7500 was corrected for using the same procedure as described in Sahleé et al. (2007). In the following, we consider fluxes from the lake to the atmosphere as positive. Data within wind directions between 040° and 200° were excluded from further analysis to avoid direct land effects and flow distortion from the mast.

Measurements made at a certain height represent properties of the underlying surface upwind of the sensor. This effective area is called the flux footprint. The footprint for the presented set-up was determined following Kljun et al. (2015), which is based on a Largrangian stochastic particle dispersion model (Kljun et al. 2002). The footprint model confirms that, for conditions within the above-mentioned wind-direction range, 80% of the source area covered by the eddy-covariance measurements at the instrument tower represent lake properties.

2.3 Method for Identification of Non-local Influence

In order to detect non-local processes, a statistical analysis, which only uses surface-layer data, is chosen. For this task, van de Boer et al. (2014) suggest an investigation of the distribution of the high-frequency humidity data. When non-local processes prevail, the humidity distribution is expected to be negatively skewed. This is the case because drier air from the free atmosphere or the outside of an internal boundary layer is entrained into the (internal) boundary layer. Additionally, drier air can be horizontally advected from the land to the lake (Fig. 3c). The skewness is a measure of the asymmetry of the humidity distribution. It is defined as the third central moment of the data divided by the cube of its standard deviation. When local processes dominate, the humidity distribution is expected to be positively skewed because the moister air from the lake reaches the boundary layer (Fig. 3a). In situations of both non-local and local processes, the distribution is expected to

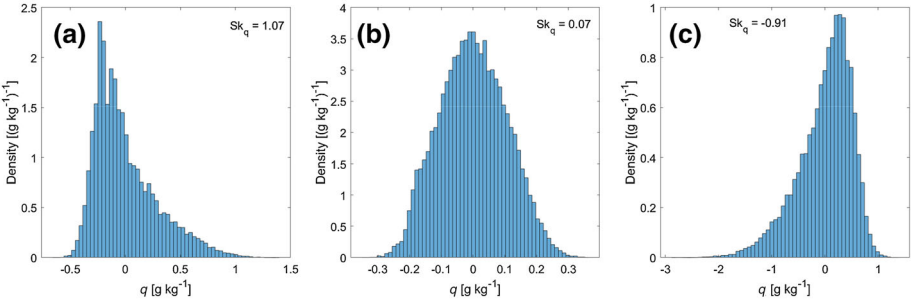

Fig. 3 Example distribution of normalized q for 1-h intervals for **a** a clearly positively skewed situation (local effects dominate), **b** a low skewness situation (non-local and local effects), and **c** a clearly negatively skewed situation (non-local effects dominate). The respective skewness parameter Sk_q is given

have low skewness (Fig. 3b), which could also be the case of a well-mixed layer. We decided to use the variance of water vapour and not CO_2 to investigate the dominating processes due to the stronger signal in the water vapour measurement. In case of CO_2, the residual layer or the free troposphere can be characterized by different CO_2 concentrations, which can either enhance or dilute the CO_2 levels in the boundary layer. Thus, CO_2 shows a less explicit signal.

The approach of van de Boer et al. (2014) cannot distinguish between vertical and horizontal humidity gradients. Thus, a negatively skewed distribution can be caused by either entrainment of dry air from the free atmosphere or by advection of dry air from the land to the flux mast. Thus, in the following, we will refer to non-local processes when a negative skewness occurs. Following van de Boer et al. (2014), the skewness was calculated for distributions of the 20-Hz humidity data over an hour. In cases of a multimodal distribution of q or a uniform distribution of q, the skewness, Sk_q, of the respective hour was removed from the further analysis. After the data processing, quality assessment, and the skewness investigation 4189 values of hourly data remain for the analysis of this study. From the remaining data, 23.5% fall into the ice-covered periods and 76.5% into the open-water periods.

2.4 Quadrant Analysis

For a further investigation of the flux contributions, we apply the quadrant analysis. This conditional sampling analysis separates the flux into four different categories based on two turbulent quantities. Here, the two fluctuating quantities are the vertical velocity component, W', and the CO_2 concentration, c'. The quadrants represent the modes of the turbulent transport. We follow the definition for the quadrants as they were used in Katul et al. (1997) and Sahleé et al. (2008): contributions to the CO_2 flux by upward-transported air where c' is positive (ejections) are obtained from quadrant I, and by downward-transported air where c' is negative (sweeps) from quadrant III.

To determine the contribution that events from a specific quadrant have on the total flux over a finite time, the (w, c)-plane can be divided by introducing a hyperbolic hole (Willmarth and Lu 1974). The hyperbolic hole is the region in the central part of the plane and is the region that is excluded from the quadrant analysis. The hole can be defined as $|w'c'| = \text{constant}$ curves, where the size of the hole H is defined as

$$H = \frac{|w'c'|}{\overline{|w'c'|}}, \tag{2}$$

so that the point (w', c') lies on the hyperbola that bounds the hole region in the (w, c)-plane. By stepwise increasing of the magnitude of H, the importance of events with increasingly large values of $\left|w'c'\right|$ can be determined in each quadrant.

The flux fraction $S_{i,H}$ of each quadrant i can be defined following Raupach (1981) as

$$S_{i,H} = \frac{[w'c']_{i,H}}{\overline{w'c'}}, \tag{3}$$

where the brackets show a conditional average, which is defined using a conditioning function $I_{i,H}$ that obeys $I_{i,H} = 1$ if the point lies in the ith quadrant and $\left|w'c'\right| \geq H = 0$ otherwise.

The flux fractions are normalized, so that

$$\sum_{i=4}^{4} = S_{i,0} = 1. \tag{4}$$

We performed the analysis for the same data as the skewness analysis. Again, we separated the data in ice-covered and open-water periods. Obvious outliers were excluded from the analysis.

3 Results

3.1 Local and Non-local Effects on Skewness and Fluxes

For both the ice-covered and open-water periods, F_{CO_2} shows a dependency on Sk_q (Fig. 4). The flux–skewness scatter is, however, different for both periods. For the ice-covered periods, the highest fluxes coincide with negative values of Sk_q and highest wind speeds ($U_{10} > 6$ m s^{-1}). As discussed above, a negative humidity skewness or one close to zero indicates that drier air from the free atmosphere or surrounding land reaches the site. This dry air adds variance to the dry side of the humidity distribution. During the ice-covered periods, only a small amount of data falls in the positive range of Sk_q, whereby most of it stays below Sk_q of 0.5 (Fig. 4a). Hence, the flux–skewness scatter plot in Fig. 4a suggests the origin of the unexpected CO_2 fluxes observed during the ice-covered periods: non-local processes.

In the following, we will investigate whether the non-local processes also affect the fluxes, which were measured during the open-water periods. For the open-water periods, the highest fluxes were higher than those observed during the ice-covered periods. The highest F_{CO_2} (values) coincide with the highest positive Sk_q (Sk_q above 0.6) and medium-range wind speeds (U_{10} around 6–9 m s^{-1}) (Fig. 4b). High positive values of Sk_q indicate the dominance of local surface-layer processes. Still, some data fall into a neutral or negative range of Sk_q. In this range, the highest F_{CO_2} (values) reach 2.5 µmol m^{-2} s^{-1} and coincide with U_{10} above 8 m s^{-1} (Fig. 4b). In this Sk_q-range, the flux-skewness scatter resembles the one observed for the ice-covered periods. The level of F_{CO_2} is similar to the one observed during the ice-covered periods. Thus, the flux–skewness scatter plot for the open-water periods indicates a combination of non-local and local processes.

When clustering the flux-skewness scatter plot in Fig. 4a, b per wind speed interval, it shows more clearly that for both the ice-covered and the open-water periods, the Sk_q decreases with increasing F_{CO_2} and increasing U_{10} (Fig. 4c, d). The main differences are (i) the level of F_{CO_2} value, which is lower for the ice-covered periods than for the open-water ones, and (ii) the values of Sk_q, which are mainly negative for the ice-covered and positive for the free-water periods. For the ice-covered periods, F_{CO_2} increases linearly with Sk_q for U_{10} above

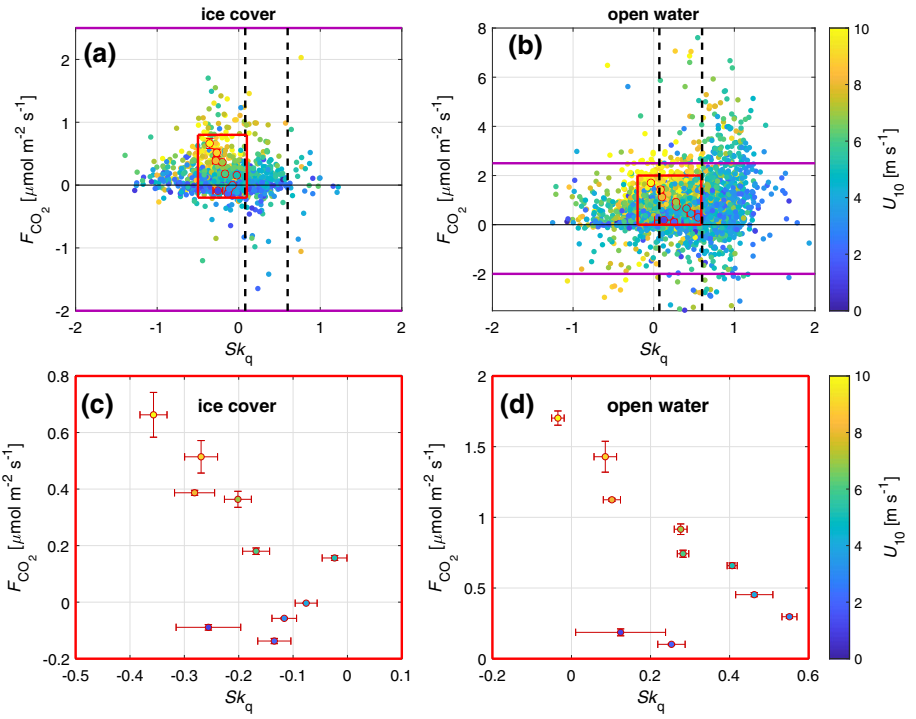

Fig. 4 Skewness versus CO_2 flux with the colour coding representing U_{10} for **a** ice-covered and **b** open-water conditions. The range of F_{CO_2} on the *y*-axis is different for **a**, **b**. The range of the ice-covered fluxes is denoted by horizontal purple lines in **b**. The vertical dashed lines show the Sk_q-thresholds for non-locally and locally dominated processes as defined in Fig. 6. The red circles in **a**, **b** show the data binned according to the wind speed level. This binned data is also shown in the same set-up but zoomed-in in **c** for ice-covered, and **d** open-water conditions. The zoomed-in windows are highlighted as red squares in **a**, **b** respectively. The error bars show the standard error

5 m s^{-1} (Fig. 4c). Thus, the highest fluxes are caused by a high level of non-local processes, which occur when wind speeds are highest. This is similar for the open-water periods, for which the fluxes begin to increase linearly with Sk_q for U_{10} above 2 m s^{-1} (Fig. 4d). At times of lowest winds, only local surface processes are important. For wind speeds above 7 m s^{-1}, however, values of Sk_q close to zero are observed. Thus, for increasing wind speeds, the effect of non-local processes gains importance and increases the flux estimations relative to the effect of only locally-driven fluxes. The fluxes that coincide with the lowest wind speeds do not follow the linear trend between U_{10}, Sk_q, and F_{CO_2}. These FCO2 values fall below 0.2 μmol m^{-2} s^{-1}. Instrumental limitations to resolve very small CO_2 fluxes are suggested for the deviations.

In Fig. 5 the contributions by ejections and sweeps to the total F_{CO_2} are shown in quadrant I and III, respectively. Similar to the skewness analysis in Fig. 4, the analysis is divided into ice-covered (Fig. 5a) and open-water periods (Fig. 5b). For both conditions, the data are divided into cases when the humidity data were positively ($Sk_q > 0$) and negatively ($Sk_q < 0$) skewed. The contribution of ejections to the total F_{CO_2} is similar for positively and negatively skewed humidity cases, during the ice-covered and open-water conditions. The contribution of sweeps, however, is larger for cases with a negative Sk_q than for cases with a positive Sk_q. Overall, the contribution of sweeps to the total F_{CO_2} is larger for the ice-

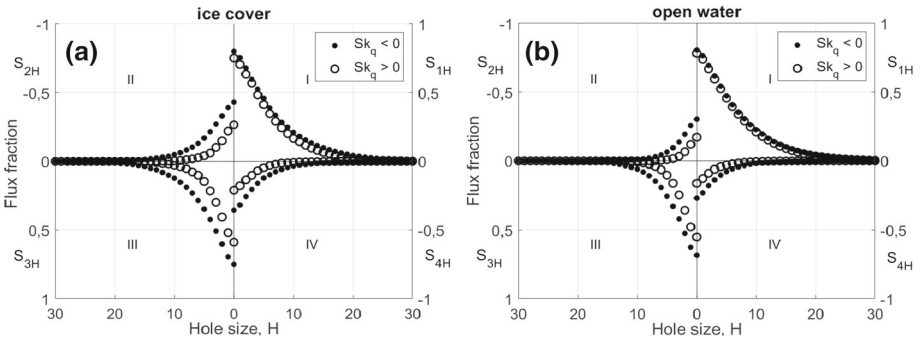

Fig. 5 Quadrant analysis of the F_{CO_2} flux for **a** ice-covered and **b** open-water conditions. Each quadrant (I–IV) represents the flux fraction $S_{i,H}$ as a function of hole size, H. The data with a positive humidity skewness ($Sk_q > 0$) are shown in black and the data with a negative humidity skewness ($Sk_q < 0$) are shown as circles

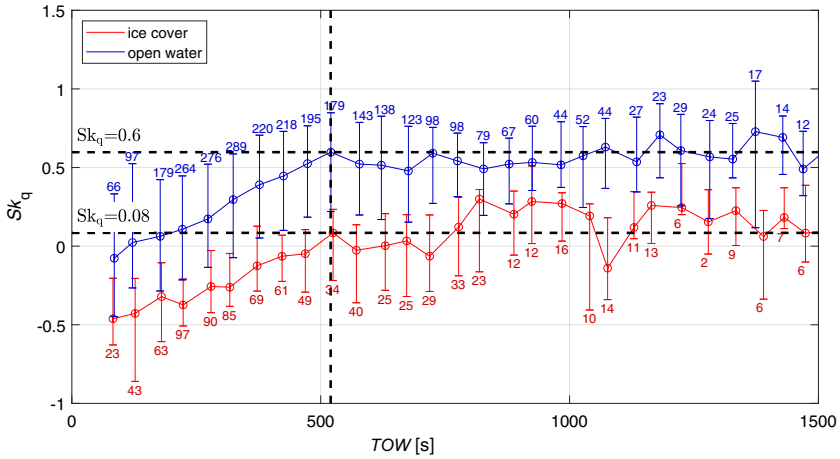

Fig. 6 Bin-averaged time over water (TOW) versus humidity skewness (Sk_q) for ice-covered (red) and open-water conditions (blue). The error bars give the 25 and 75 percentiles. The numbers at the error bars indicate the amount of samples in each bin. The horizontal and vertical dashed lines give the Sk_q and TOW at which the relations level off. These thresholds are indicated in Fig. 4 by the vertical dashed lines

covered conditions than for the open-water-conditions for a wide range of H. This supports the conclusions that cases of negative Sk_q represent non-local contributions to the total CO_2 flux that were carried to the lake from above. The quadrant analysis can only investigate vertical contributions to the total flux. Thus, it ignores any horizontal contributions.

The scatter plot of flux versus skewness in Fig. 4 shows the increasing importance of non-local processes with increasing U_{10}. However, the occurrence of non-local processes may not only depend on U_{10} but rather a combination of U_{10} and the prevailing fetch. The fetch is defined as the distance from the instrumented tower to the shore in the upwind direction. We can express this transported distance as time over water with $TOW = \frac{\text{fetch}}{U_{10}}$. Figure 6 shows the bin averaged TOW versus Sk_q for the ice-covered and open-water periods. For the ice-covered period, the level of Sk_q increases with increasing TOW until it levels off at $Sk_q = 0.08$ and TOW of 520 s. The point of the levelling-off is determined as the point at which two fitted linear curves to the data above and below have the largest difference in

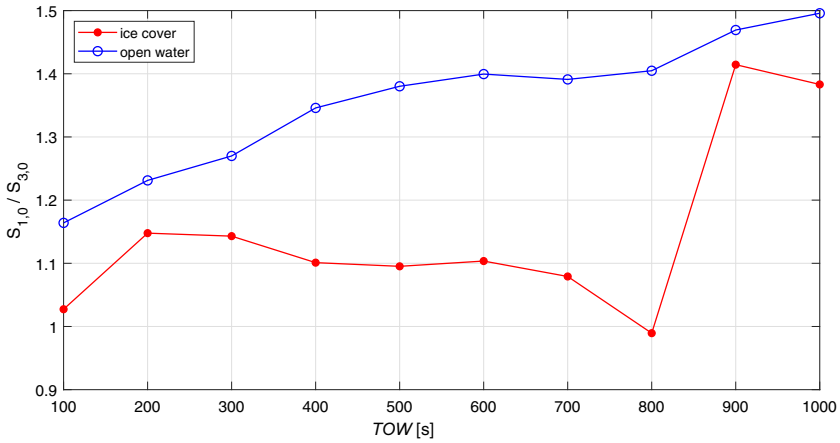

Fig. 7 Time over water (*TOW*) versus the ratio of the first to third quadrant for a hole size of zero ($S_{1,0}/S_{3,0}$) for ice-covered (red) and open-water conditions (blue)

their slopes. Similarly for the open-water period, the level of Sk_q increases with increasing *TOW* and levels off at $Sk_q = 0.60$ and *TOW* of 520 s. The Sk_q for the free-water periods passes zero at $TOW = 185$ s. A dependency of Sk_q on *TOW* is only expected when non-local processes influence the fluxes.

The ratio of the contributions to the total F_{CO_2} from ejections and sweeps can be expressed as the ratio of the first and third quadrant of the quadrant analysis for a specific hole size, $S_{1,i}/S_{3,i}$. Figure 7 shows this ratio (i.e., the contribution of all sweep and ejection events) for a hole size of zero versus the *TOW* for the ice-covered (blue) and open-water conditions (blue). For all *TOW*, the ratio $S_{1,0}/S_{3,0}$ of the open-water conditions is above 1. Hence, the contributions to the total F_{CO_2} from below are larger than those from above. For the smallest *TOW*, the ratio falls closest to unity and increases with increasing *TOW*. Thus, with increasing *TOW* the contributions from sweeps lessen in importance. Comparing the relation of Sk_q versus *TOW* to the $S_{1,0}/S_{3,0}$ versus *TOW*, for open-water conditions, shows that both relations follow a similar shape and level off in a *TOW* range between 500 and 600 s. This suggests that we can relate the described non-local impacts to flux contributions that reach the site from above.

For all *TOW*, the ratio of $S_{1,0}/S_{3,0}$ is smaller for the ice-covered than for the open-water conditions. As expected from our previous findings, the flux contributions from sweeps are more dominant for the ice-covered conditions. Below a *TOW* of 800 s the $S_{1,0}/S_{3,0}$ stays in a range between 1 and 1.15. Only at *TOW* above 800 s does the ratio increase to values of 1.4 and contributions from below gain importance. This is the same range of *TOW* at which the Sk_q in the Sk_q versus *TOW* relation changes sign from negative to positive and eventually passes the threshold of $Sk_q = 0.08$ (in Fig 6).

3.2 Flux Correction

The relation between *TOW* and Sk_q in Fig. 6 can be used to define thresholds for the regimes in which non-local or local processes dominate. These thresholds allow for dividing the fluxes into

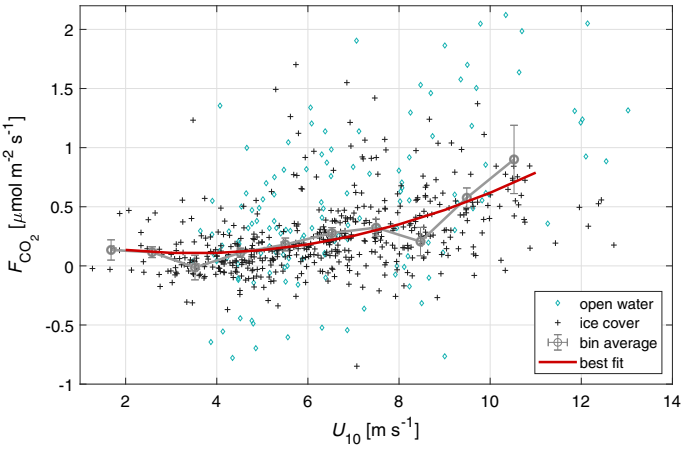

Fig. 8 Wind speed versus F_{CO_2} for the situations that are determined to be dominantly non-locally driven. $F_{\mathrm{non-local}}$ during ice-covered periods is shown as blue diamonds and during open-water periods as black crosses. The data of both ice and no-ice conditions are bin-averaged and the error bars show the standard error (grey). The best fit through the combined data is shown in red

$$F = \begin{cases} F_{\mathrm{local}} = F(Sk_q > 0.60 \;\&\; TOW > 520\mathrm{s}) \\ F_{\mathrm{both}} = F(0.08 < Sk_q < 0.60 \;\&\; TOW < 520\mathrm{s}) \\ F_{\mathrm{non-local}} = F(Sk_q < 0.08 \;\&\; TOW < 520\mathrm{s}) \end{cases} . \tag{5}$$

To gain accurate estimates of the air–lake gas exchange rates, the non-local effects should be filtered out from the measured eddy-covariance fluxes. Such a correction of the measured fluxes for the non-local processes forms Eq. 5 into:

$$F_{\mathrm{corr}} = \begin{cases} F_{\mathrm{local}} \\ F_{\mathrm{both}} - F_{\mathrm{non-local}} \\ 0 \end{cases} . \tag{6}$$

The flux separation in Eq. 5 allows for a wind-speed based parametrization of the fluxes that are generated by non-local effects (Fig. 8). Figure 8 shows the $F_{\mathrm{non-local}}$, as defined in Eq. 5, versus wind speed for both the ice-covered (black crosses) and open-water (blue diamonds) conditions. This definition of $F_{\mathrm{non-local}}$ covers 628 hourly data points. A quadratic least-square fit through both the ice-covered and open-water periods explains 55.3% of the data's variance (the adjusted coefficient of determination is 0.553). This fit follows the fluxes that are bin-averaged according to wind speed. This expression of the non-local fluxes [μ mol m^{-2} s^{-1}] as a function of wind speed is given by

$$F_{\mathrm{non-local}}(U_{10}) = 0.0122\, U_{10}^2 - 0.0860\, U_{10} + 0.2580 \tag{7}$$

In a next step, $F_{\mathrm{non-local}}$ is subtracted from the eddy-covariance fluxes that fall within the limits of F_{both} and $F_{\mathrm{non-local}}$. Figure 9 shows the original (grey) and corrected (red) estimates of F_{CO_2} bin-averaged according to U_{10}, separately for ice-covered and open-water periods. For the ice-covered periods, F_{corr} falls close to zero for all U_{10} compared to the original F_{CO_2}. For U_{10} below 8 m s^{-1} the bin-averaged F_{corr} are zero (within the range of the standard error); for U_{10} above 8 m s^{-1} they are in a range of $-0.2\,\mu$mol m^{-2} s^{-1}, thus

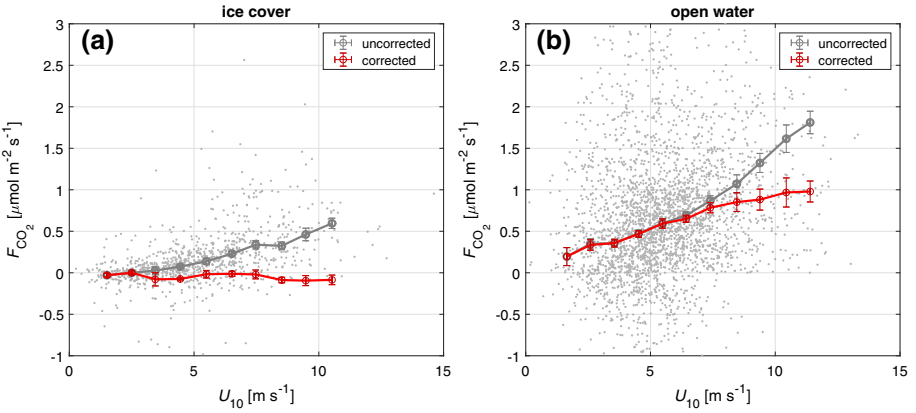

Fig. 9 Wind speed versus F_{CO_2} for all data of **a** ice-covered and **b** open-water situations. The fits represent the 1 m s^{-1} bin-averaged data (gray) and the bin-averages of the corrected flux based on the fits in Fig. 8 (red). The error bars give the standard error

minimally overcorrected since the best fit included both open-water and ice-covered periods. Less high-wind-speed data is available, which is reflected in the larger standard errors. For the open-water periods, the bin-averaged F_{corr} follows the original F_{CO_2} for U_{10} below 5 m s^{-1} and shows a significant reduction for higher U_{10}.

3.3 Gas Transfer Velocity

The measured F_{CO_2} allows for calculating the gas transfer velocity for the open-water periods following Eq. 1. For this, simultaneous measurements of CO_2 partial pressure at the water surface are used. This reduced the number of available data to 673 hourly values. When estimating k only local effects are relevant, and thus non-local effects should be removed. The elimination of non-local effects on F_{CO_2} is reflected in the resulting values of k. Figure 10 shows the bin-averaged k normalized to a Schmidt number, Sc, of 600, which reflects CO_2 at 20°, based on the corrected (red) and uncorrected (grey) F_{CO_2}. The elimination of the non-local effects reduces the estimations of the uncorrected k. This reduction increases with increasing wind speed. At a wind speed of 12 m s^{-1}, the correction reduces the original k by almost 50%.

For comparison, k was calculated from some frequently applied wind-based models by McGillis et al. (2001)

$$k_{MG01} = 3.3 + 0.026\, U_{10}^3 (Sc/660)^{-0.5}, \tag{8}$$

by Wanninkhof (1992)

$$k_{W92} = 0.31\, U_{10}^2 (Sc/660)^{-0.5}, \tag{9}$$

by Nightingale et al. (2000)

$$k_{N00} = 0.222\, U_{10}^2 + 0.333\, U_{10}, \tag{10}$$

and by Cole and Caraco (1998)

$$k_{CC98} = 2.07 + 0.215 U_{10}^{1.7}. \tag{11}$$

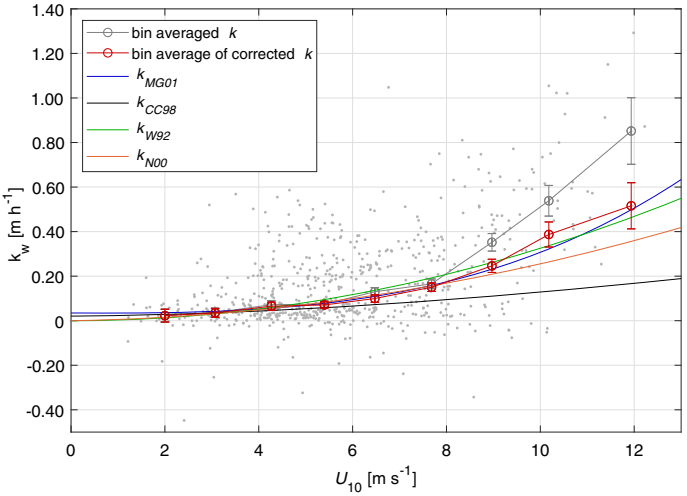

Fig. 10 Wind speed versus the gas transfer velocity, k, determined from the fluxes during open-water situations. The fits represent the 1 $\mathrm{m\,s^{-1}}$ bin-averaged data (grey) and the bin-averages of the k determined from the corrected flux (red). The error bars give the standard error. Also, commonly used wind speed based parametrizations by McGillis et al. (2001) (k_{MG01}), Cole and Caraco (1998) (k_{CC98}), Wanninkhof (1992) (k_{W92}), and Nightingale et al. (2000) (k_{N00}) are shown

In general, the corrected k follow these frequently applied parametrizations better than the uncorrected k. Among these parametrizations k_{MG01} describes the corrected k best. The expressions for k_{MG01}, k_{W92}, and k_{N00} are empirical relations, which are based on ocean observations. In contrast to k_{W92} and k_{N00}, k_{MG01} accounts for buoyancy effects, chemical enhancement, surface waves, and micro breaking events by adding a constant value of k. This forces gas exchange to occur even at low wind speeds. At higher wind speeds, the corrected k is still significantly higher than the values predicted by Cole and Caraco (1998), a frequently used transfer velocity parametrization for lakes, derived from SF6 tracer experiment.

4 Discussion

4.1 Origin of Eddy-Covariance Fluxes During Ice-Covered Periods

Neither the quadrant analysis nor the statistical method that we used in this study can explicitly distinguish whether horizontal or vertical processes cause the enhanced variance on the dry side of the humidity distribution. The additional dry air in situations of non-local processes could either be entrained to the (internal) boundary layer from the free atmosphere or the mixed or residual layer depending on the stratification, or advected from the surrounding land. This study aimed to present a method to identify and correct for the effects of these non-local processes on eddy-covariance flux measurements. A distinction between the different types of non-local processes is beyond the scope of this study and may require additional new data including vertical profiles of humidity and other variables (e.g., from radiosoundings or UAV measurements).

4.2 Implications for Eddy-Covariance Lake Studies

Figure 6 shows that non-local processes affect lakes up to a *TOW* of 520 s. This threshold allows for determining the smallest fetch at a given wind speed for which CO_2 fluxes from/to a specific lake are affected by such non-local processes. For example, for a maximal wind speed of 10 $m\,s^{-1}$, a minimal fetch of 5200 m was required for lake fluxes to be independent of non-local effects. Such concepts are particularly important because many of the existing eddy-covariance studies on lakes are conducted at rather small lakes. According to the fetches of these lakes and the reported wind speeds, some of the air–lake fluxes are expected to always be affected by differently pronounced non-local processes [e.g. Lake Villasjön (Jammet et al. 2017), Lake Soppensee (Eugster et al. 2003), Lake Toolik (Eugster et al. 2003), or Lake Valkea-Kotinen (Vesala et al. 2006)]. For other lakes with longer fetch and/or lower reported wind speed, the fluxes might either be affected by non-local processes only under specific conditions or not at all [e.g., Lake Kuivajärvi (Heiskanen et al. 2014; Mammarella et al. 2015; Erkkilä et al. 2018) and Lake Tämnaren (Sahleé et al. 2014; Podgrajsek et al. 2015)]. The non-local processes do not depend on the surface size but rather the distance between the eddy-covariance mast and the shore in the direction of the wind.

Our analysis follows those of Barskov et al. (2019) for heat exchange between a frozen lake and the atmosphere, who found that heat and momentum fluxes are primarily forced due to local surface processes when the flow is from an adjacent gulf (long fetch). When the wind comes from directions of a surrounding forest (short fetch), Barskov et al. (2019) observed a significant increase in their eddy-covariance fluxes, while the estimates from Monin–Obukhov similarity theory nearly vanish. Similarly, the method presented here would, for the given fetch and wind speeds, suggest non-local processes as a primary driver for the observed fluxes.

4.3 Gas Transfer Velocity

The uncorrected gas transfer velocity overestimates the predictions from frequently used wind-based parametrizations, in particular for wind speeds above 8 $m\,s^{-1}$. This overestimation due to non-local flux contributions is reduced for k determined from the corrected fluxes. The corrected k follow the parametrization by McGillis et al. (2001) (k_{MG01}) closest. Still, for wind speeds above 7 $m\,s^{-1}$ the corrected k are higher than the predictions from Cole and Caraco (1998) (k_{CC98}), which were developed for lakes. Other studies from lakes found higher values for k than those derived from SF_6 in Cole and Caraco (1998) (e.g., Jonsson et al. 2008; Heiskanen et al. 2014; Mammarella et al. 2015). This follows eddy-covariance studies from the ocean, which reported higher values for k than from other methods (e.g., McGillis et al. 2004). Thus, upscaling CO_2 emissions from lakes based on k_{CC98} will likely underestimate the actual emissions. At wind speeds of 12 $m\,s^{-1}$, we observed 50% higher fluxes than predicted by k_{CC98}. Such an overestimation can gain a significant impact on the global carbon contribution from lakes to the atmosphere. Hence, it is important to separate local and non-local flux contributions to the total lake–air exchange when possible. Other studies have shown that parametrizations of k that include other factors than wind speed alone gain improved results (e.g., Rutgersson et al. 2011; Heiskanen et al. 2014; Podgrajsek et al. 2015; Esters et al. 2017). These additional factors include, for example, buoyancy effects, or are directly related to water-side turbulence.

5 Conclusions

The unexpected air–water CO_2 fluxes observed during ice-covered and also open-water seasons in Lake Erken have been investigated. Using the statistical method of van de Boer et al. (2014) we identified the origin of these fluxes as non-local processes. The findings were supported by the quadrant analysis, which related the non-local processes to flux contributions from above. The occurrence and strength of these non-local processes depend on a combination of wind speed and fetch, expressed as the time over water (*TOW*). The shorter the fetch and the greater the wind speed, the more strongly non-local processes affect the observed eddy-covariance CO_2 fluxes. The limits for the dominance of non-local processes was formulated based on the time over water and the humidity skewness as $Sk_q < 0.08$ and $TOW < 520$ s. The limits for the dominance of local surface processes was determined as $Sk_q > 0.60$ and $TOW > 520$ s. Scenarios in between these limits reflect fluxes that are influenced by local and non-local processes. The analysis suggests to correct eddy-covariance fluxes from lakes for the non-local effects. All fluxes not falling into the limits of dominantly surface-driven fluxes should be subtracted by $F_{\mathrm{non-local}}(U_{10}) = 0.0122\,U_{10}^2 - 0.0860\,U_{10} + 0.2580$ [μmol $\mathrm{m}^{-2}\,\mathrm{s}^{-1}$]. This expression describes the purely non-locally driven fluxes. Correcting the CO_2 fluxes for non-local effects leads to a reduction in the observed gas transfer velocity. The reduced values of k followed commonly used wind-based parametrizations for k derived for open-ocean conditions with long to essentially unlimited fetch. The proposed analysis methods, illustrated here with Lake Erken data, are potentially of great importance for better quantification of the exchange of carbon between lakes and inland freshwater bodies to the atmosphere, which is a well-known open scientific question of the global carbon cycle.

Acknowledgements We thank the staff of the Erken laboratory who greatly assisted the data acquisition. The study was supported by funding from the Knut and Alice Wallenberg foundation (KAW 2013.0091). The measurements and the Erken station is one component within the national infrastructure SITES (Swedish Infrastructure for Ecosystem Science).

Funding Open access funding provided by Uppsala University.

Open Access This article is licensed under a Creative Commons Attribution 4.0 International License, which permits use, sharing, adaptation, distribution and reproduction in any medium or format, as long as you give appropriate credit to the original author(s) and the source, provide a link to the Creative Commons licence, and indicate if changes were made. The images or other third party material in this article are included in the article's Creative Commons licence, unless indicated otherwise in a credit line to the material. If material is not included in the article's Creative Commons licence and your intended use is not permitted by statutory regulation or exceeds the permitted use, you will need to obtain permission directly from the copyright holder. To view a copy of this licence, visit http://creativecommons.org/licenses/by/4.0/.

References

Asanuma J, Tamagawa I, Ishikawa H, Ma Y, Hayashi T, Qi Y, Wang J (2007) Spectral similarity between scalars at very low frequencies in the unstable atmospheric surface layerover the Tibetan plateau. Boundary-Layer Meteorol 122:85–103. https://doi.org/10.1007/s10546-006-9096-y

Aubinet M, Berbigier P, Bernhofer CH, Cescatti A, Feigenwinter C, Granier A, Grünwald T, Havrankova K, Heinesch B, Longdoz B, Marcolla B, Montagnani L, Sedlak P (2005) Comparing CO_2 storage and advection conditions at night at different carboeuroflux sites. Boundary-Layer Meteorol 116:63–93. https://doi.org/10.1007/s10546-004-7091-8

Aubinet M, Vesala T, Papale D (2012) Eddy covariance: a practical guide to measurement and data analysis. Springer, New York

Baldocchi DD, Meyers TP (1988) Turbulence structure in a deciduous forest. Boundary-Layer Meteorol 43(4):345–364. https://doi.org/10.1007/BF00121712

Baldocchi DD, Vogel CA (1996) Energy and CO_2 flux densities above and below a temperate broad-leaved forest and a boreal pine forest. Tree Physiol 16:5–16. https://doi.org/10.1093/treephys/16.1-2.5

Barskov K, Stepanenko V, Repina I, Artanmonov A, Gavrikov A (2019) Two regimes of turbulent fluxes above a frozen small lake surrounded by forest. Boundary-Layer Meteorol 173:311–320. https://doi.org/10.1007/s10546-019-00469-w

van de Boer A, Moene A, Graf A, Schüttemeyer D, Simmer C (2014) Detection of entrainment influences on surface-layer measurements and extension of Monin–Obukhov similarity theory. Boundary-Layer Meteorol 152:19–44. https://doi.org/10.1007/s10546-014-9920-8

Bruin HD, Kohsiek W, van den Hurk J (1993) A verification of some methods to determine the fluxes of momentum, sensible heat, and water vapour using standard deviation and structure parameter of scalar meteorological quantities. Boundary-Layer Meteorol 63:231–257

Bruin HD, van den Hurk J, Kroon LJM (1999) On the temperature–humidity correlation and similarity. Boundary-Layer Meteorol 93:453–468

Choi T, Hong J, Kim J, Lee H, Asanuma J, Ishikawa H, Tsukamoto O, Zhiqiu G, Ma Y, Ueno K, Wang J, Koike T, Yasunari T (2004) Turbulent exchange of heat, water vapor, and momentum over a Tibetan prairie by eddy covariance and flux variance measurements. J Geophys Res 109(D21):106. https://doi.org/10.1029/2004JD004767

Cole JJ, Caraco NF (1998) Atmospheric exchange of carbon dioxide in a low-wind oligothrophic lake measured by the addition of SF6. Limnol Oceanogr 43:647–656

Cole JJ, Praire YT, Caraco NF, McDowell WH, Tranvik LJ, Striegl RG, Duarte MC, Kortelainen P, Downing JA, Middelburg JJ, Melack J (2007) Plumbing the global carbon cycle: integrating inland waters into the terrestrial carbon budget. Ecosystems 10:172–185. https://doi.org/10.1007/s10021-006-9013-8

Dabberdt WF, Lenschow DH, Horst TW, Zimmermann PR, Oncley SP, Delany AC (1993) Atmosphere–surface exchange measurements. Science 260(5113):1472–1481. https://doi.org/10.1126/science.260.5113.1472

Erkkilä KM, Ojala A, Bastviken D, Biermann T, Heiskanen JJ, Lindroth A, Peltola O, Rantakari M, Vesala T, Mammarella I (2018) Methane and carbon dioxide fluxes over a lake: comparison between eddy covariance, floating chambers and boundary layer method. Biogeosciences 15:429–445. https://doi.org/10.5194/bg-15-429-2018

Esters L, Landwehr S, Sutherland G, Bell TG, Christensen KH, Saltzman ES, Miller SD, Ward B (2017) Parameterizing air-sea gas transfer velocity with dissipation. J Geophys Res Oceans 122:3041–3056. https://doi.org/10.1002/2016JC012088

Eugster W, Kling GW, Jonas T, McFadden JP, Wuest A, MacIntyre S III, SFC, (2003) CO_2 exchange between air and water in an Arctic Alaskan and midlatitude Swiss lake: importance of convective mixing. J Geophys Res 108:4362. https://doi.org/10.1029/2002JD002653

Feigenwinter C, Bernhofer C, Vogt R (2004) The influence of advection on the short term CO_2-budget in and above a forest canopy. Boundary-Layer Meteorol 113(2):201–224. https://doi.org/10.1023/B:BOUN.0000039372.86053.ff

Gao Z, Liu H, Li D, Katul GG, Blanken PD (2018) Enhanced temperature–humidity similarity caused by entrainment processes with increased wind shear. J Geophys Res Atmos 123:4110–4121. https://doi.org/10.1029/2017JD028195

Heiskanen JJ, Mammarella I, Haapanala S, Pumpanen J, Vesala T, MacIntyre S, Ojala A (2014) Effects of cooling and internal wave motions on gastransfer coefficients in a boreal lake. Tellus Ser B Chem Phys Meteorol 66(22):827. https://doi.org/10.3402/tellusb.v66.22827

Higgins CW, Pardyjak E, Froidevaux M, Simeonov V, Parlange MB (2013) Measured and estimated water vapor advection in the atmospheric surface layer. J Hydrometeorol 14(6):1966–1972. https://doi.org/10.1175/JHM-D-12-0166.1

Horst T, Lenschow D (2009) Attenuation of scalar fluxes measured with spatially displaced sensors. Boundary-Layer Meteorol 130:275–300. https://doi.org/10.1007/s10546-008-9348-0

Huang J, Lee X, Patton EG (2008) A modelling study of flux imbalance and the influence of entrainment in the convective boundary layer. Boundary-Layer Meteorol 127:273–292. https://doi.org/10.1007/s10536-007-9254-x

Huotari J, Ojala A, Peltomaa E, Nordbo A, Launiainen S, Pumpanen J, Rasilo T, Hari P, Vesala T (2011) Long-term direct CO_2 flux measurements over a boreal lake: five years of eddy covariance data. Geophys Res Lett. https://doi.org/10.1029/2011GL048753

Jammet M, Dengel S, Kettner E, Parmentier FJW, Wik M, Crill P, Friborg T (2017) Year-round CH_4 and CO_2 flux dynamics in two contrasting freshwater ecosystems of the subarctic. Biogeosciences 14:5189–5216. https://doi.org/10.5194/bg-14-5189-2017

Jonsson A, Aberg J, Lindroth A, Jansson M (2008) Gas tranfer rate and CO_2 flux between an unproductive lake and the atmosphere in northern Sweden. J Geophys Res 113(G04):006. https://doi.org/10.1029/2008JG000688

Kaimal JC, Finnigan JJ (1994) Amospheric boundary layer flows: their structure and measurement. Oxford University Press, Oxford

Katul GG, Schieldge J, Hsieh C-I (1997) The ejection–sweep character of scalar fluxes in the unstable surface layer. Boundary-Layer Meteorol 83:1–26

Katul GG, Sempreviva AM, Cava D (2008) The temperature–humidity covariance in the marine surface layer: a one-dimensional analytical model. Boundary-Layer Meteorol 126:263–278. https://doi.org/10.1007/s10546-007-9236-z

Kenny WT, Bohrer G, Morin TH, Vogel CS, Matheny AM, Desai AR (2017) A numerical case study of the implications of secondary circulations to the interpretation of eddy-covariance measurements over small lakes. Boundary-Layer Meteorol 165:311–332. https://doi.org/10.1007/s10546-017-0268-8

Kljun N, Rotach MW, Schmid HP (2002) A 3-D backward Lagrangian footprint model for a wide range of boundary layer stratifications. Boundary-Layer Meteorol 103(2):205–226. https://doi.org/10.1023/A:1014556300021

Kljun N, Calanca P, Rotach MW, Schmid HP (2015) A simple two-dimensional parameterisation for Flux Footprint Prediction (FFP). Geosci Model Dev 8:3695–3713. https://doi.org/10.5194/gmd-8-3695-2015

Lee X, Law B, Massman W (2005) Handbook of micrometeorology: a guide for surface flux measurement and analysis. Springer, Dordrecht. https://doi.org/10.1007/1-4020-2265-4

Lenschow DH, Krummel PB, Siems ST (1999) Measuring entrainment, divergence, and vorticity on the mesoscale from aircraft. J Atmos Ocean Technol 16:1384–1400

Loescher HW, Law BE, Mahrt L, Hollinger DY, Campbell J, Wofsy SC (2006) Uncertainties in, and interpretation of, carbon flux estimates using the eddy covariance technique. Clim Dyn 111:DS1S90. https://doi.org/10.1029/2005JD006932

Lohou F, Saïd F, Lothon M, Durand P, Serça D (2010) Impact of boundary-layer processes on near-surface turbulence within the West African monsoon. Boundary-Layer Meteorol 136(1):1–23

Mammarella I, Nordbo A, Rannik Ü, Haapanala S, Levula J, Laakso H, Ojala A, Peltola O, Heiskanen J, Pumpanen J, Vesala T (2015) Carbon dioxide and energy fluxes over a small boreal lake in Southern Finland. J Geophys Res Biogeosci 120:1296–1314. https://doi.org/10.1002/2014JG002873

Massman W, Lee X (2002) Eddy covariance flux corrections and uncertainties in long-term studies of carbon and energy exchanges. Agric For Meteorol 113(1):121–144. https://doi.org/10.1016/S0168-1923(02)00105-3

McGillis WR, Edson JB, Hare JE, Fairall CW (2001) Direct covariance air–sea CO_2 fluxes. J Geophys Res 106:16,729–16,745

McGillis WR, Edson JB, Zappa CJ, Ware JR, McKenna SP, Terray EA, Hare JE, Fairall CW, Drennan W, Donelan M, DeGrandpre MD, Wanninkhof R, Feely RA (2004) Air–sea CO_2 exchange in the equatorial Pacific. J Geophys Res 109:C08S02. https://doi.org/10.1029/2003JC002256

Morin TH, Rey-Sánchez AC, Vogel CS, Matheny AM, Kenny WT, Bohrer G (2018) Carbon dioxide emissions from an oligotrophic temperate lake: an eddy covariance approach. Ecol Eng 114:25–33. https://doi.org/10.1016/j.ecoleng.2017.05.005

Nightingale PD, Malin G, Law CS, Watson AJ, Liss PS, Liddicoat MI, Boutin J, Upstill-Goddard RC (2000) In situ evaluation of air–sea gas exchange parameterizations using novel conservative and volatile tracers. Glob Biogeochem Cycles. https://doi.org/10.1029/1999GB900091

Nilsson EO, Rutgersson A, Sullivan P (2010) Flux attenuation due to sensor displacement over sea. J Atmos Ocean Technol 27:856–868. https://doi.org/10.1175/2010JTECHA1388.1

Podgrajsek E, Sahlée E, Bastviken D, Holst J, Lindroth A, Tranvik L, Rutgersson A (2014) Comparison of floating chamber and eddy covariance measurements of lake greenhouse gas fluxes. Biogeosciences 11:4225–4233. https://doi.org/10.5194/bg-11-4225-2014

Podgrajsek E, Sahlée E, Rutgersson A (2015) Diel cycle of lake–air CO_2 flux from a shallow lake and the impact of waterside convection on the transfer velocity. J Geophys Res Biogeosci 120:29–38

Raymond PA, Hartman J, Lauerwald R, Sobek S, Mcdonald C, Hoover M, Butman D, Striegl R, Mayorga E, Humborg C, Kortelainen P, Durr H, Meybeck M, Ciais P, Guth P (2013) Global carbon dioxide emissions from inland waters. Nature 503:355–359

Raupach MR (1981) Conditional statistics of Reynolds stress in rough-wall and smooth-wall turbulent boundary layers. J Fluid Mech 108:363–382

Rutgersson A, Smedman A, Sahleé E (2011) Oceanic convective mixing and the impact on air–sea gas transfer velocity. Geophys Res Lett 38(L02):602. https://doi.org/10.1029/2010GL045581

Sahleé E, Smedman AS, Rutgersson A, Högström U (2007) Spectra of CO_2 and water vapor in the marine atmospheric surface layer. Boundary-Layer Meteorol 126(2):279–295. https://doi.org/10.1007/s10546-007-9230-5

Sahleé E, Smedman AS, Högström U, Rutgersson A (2008) Re-evaluation of the bulk exchange coefficient for humidity at sea during unstable and neutral conditions. J Phys Oceangr 38:257–272. https://doi.org/10.1175/2007JPO3754.1

Sahleé E, Drennan WM, Potter H, Rebozo MA (2012) Waves and air–sea fluxes from a drifting ASIS buoy during the southern ocean gas exchange experiment. J Geophys Res 117:C08003. https://doi.org/10.1029/2012JC008032

Sahleé E, Rutgersson A, Podgarjsek E, Bergström H (2014) Influence from surrounding land on the turbulence measurements above a lake. Boundary-Layer Meteorol 150:235–258. https://doi.org/10.1007/s10546-013-9868-0

Spank U, Hehn M, Keller P, Koschorreck M, Bernhofer C (2019) A season of eddy-covariance fluxes above an extensive water body based on observations from a floating platform. Boundary-Layer Meteorol. https://doi.org/10.1007/s10546-019-00490-z

Sun J, Desjardins R, Mahrt L, MacPherson I (1998) Transport of carbon dioxide, water vapor, and ozone by turbulence and local circulations. J Geophs Res Atmos 103:25,873–25,885. https://doi.org/10.1029/98JD02439

Tranvik LJ, Downing JA, Cotner JB, Loiselle SA, Striegl RG, Ballatore TJ, Dillon P, Finlay K, Fortino K, Knoll LB, Kortelainen PL, Kutser T, Larsen S, Laurion I, Leech DM, McCallister SL, McKnight DM, Melack JM, Overholt E, Porter JA, Prairie Y, Renwick WH, Roland F, Sherman BS, Schindler DW, Sobek S, Tremblay A, Vanni MJ, Verschoor AM, von Wachenfeldt E, Weyhenmeyer GA (2009) Lakes and reservoirs as regulators of carbon cycling and climate. Limnol Oceanogr 54:2298–2314. https://doi.org/10.4319/lo.2009.54.6_part_2.2298

Vesala T, Huotari J, Rannik Ü, Suni T, Smolander S, Sogachev A, Launiainen S, Ojala A (2006) Eddy covariance measurements of carbon exchange and latent and sensible heat fluxes over a boreal lake for a full open-water period. J Geophys Res 111(D11):101. https://doi.org/10.1029/2005JD006365

Wanninkhof R (1992) Relationship between wind speed and gas exchange over the ocean. J Geophys Res 97(C5):7373–7382. https://doi.org/10.1029/92JC00188

Webb EK, Pearman GI, Leuning R (1980) Correction of flux measurements for density effects due to heat and water vapour transfer. Q J R Meteorol Soc 106:85–100

Willmarth WW, Lu SS (1974) Structure of the Reynolds stress and the occurrence of bursts in the turbulent boundary layer. Adv Geophys 18A:287–314

Publisher's Note Springer Nature remains neutral with regard to jurisdictional claims in published maps and institutional affiliations.